Measuring Lipid Membrane Viscosity Using Rotational and Translational Probe Diffusion

Tristan T. Hormel, Sarah Q. Kurihara, M. Kathleen Brennan, Matthew C. Wozniak, and Raghuveer Parthasarathy*
Department of Physics and Materials Science Institute, University of Oregon, Eugene, Oregon 97401, USA
(Received 2 August 2013; published 6 May 2014)

The two-dimensional fluidity of lipid bilayers enables the motion of membrane-bound macromolecules and is therefore crucial to biological function. Microrheological methods that measure fluid viscosity via the translational diffusion of tracer particles are challenging to apply and interpret for membranes, due to uncertainty about the local environment of the tracers. Here, we demonstrate a new technique in which determination of both the rotational and translational diffusion coefficients of membrane-linked particles enables quantification of viscosity, measurement of the effective radii of the tracers, and assessment of theoretical models of membrane hydrodynamics. Surprisingly, we find a wide distribution of effective tracer radii, presumably due to a variable number of lipids linked to each tracer particle. Furthermore, we show for the first time that a protein involved in generating membrane curvature, the vesicle trafficking protein Sar1p, dramatically increases membrane viscosity. Using the rheological method presented here, therefore, we are able to reveal a class of previously unknown couplings between protein activity and membrane mechanics.

DOI: 10.1103/PhysRevLett.112.188101 PACS numbers: 87.14.Cc, 05.40.Jc, 83.10.Mj

Lipid membranes are two-dimensional fluids, a physical characteristic that enables individual lipids, lipid domains, embedded proteins, and macromolecular complexes to spatially reorganize and to interact with one another [1–6]. Though measurements of lipid and protein diffusion coefficients are routine, it is difficult to determine membrane viscosity, the fundamental material property that describes fluid response, from such measurements. This difficulty can be ascribed in part to ignorance of the effective size of diffusing bodies. The approach we describe here uses measurement of both the translational and rotational diffusion coefficients of membrane-anchored tracer particles to provide, via simple analysis, precise and robust values of viscosity as well as effective tracer radii. The method is generally applicable to membranes of different compositions and geometries, and allows tests of theoretical models of membrane hydrodynamics. Moreover, it enables discovery of rheological effects induced by membrane proteins. We provide the first demonstration that a protein involved in generating membrane curvature also has a large impact on the effective in-plane membrane viscosity, a finding that would have been difficult to uncover with existing techniques.

Diffusion in two dimensions is inherently nontrivial due to the long range of flow fields. Saffmann and Delbrück (SD) showed that hydrodynamic coupling between the 2D membrane and the bulk 3D fluid results in well-defined diffusive behavior within the membrane [7]. According to this model, the rotational and translational drag coefficients Λ_R and Λ_T, respectively, for a disklike membrane inclusion of radius a are given by

$$\Lambda_T = \frac{4\pi\eta_m}{\ln(2\epsilon^{-1}) - \gamma}, \tag{1}$$

$$\Lambda_R = 4\pi\eta_m a^2, \tag{2}$$

where γ is Euler's constant, η_m is the two-dimensional membrane viscosity, and $\epsilon = 2\eta_w a/\eta_m$ is a dimensionless number relating a, η_m, and the bulk 3D viscosity η_w. The diffusion coefficients follow from the drag coefficients via the Einstein relations $D_{R,T} = k_B T(\Lambda_{R,T})^{-1}$, where k_B is Boltzmann's constant and T is the temperature. The SD model is valid in the limit of small ϵ, corresponding to membrane inclusion radii that are small compared to the ratio of the 2D membrane viscosity to the 3D bulk viscosity. Hughes, Pailthorpe, and White (HPW) extended the SD model to arbitrary ϵ [8]. The full HPW model cannot be condensed into simple equations, but can be evaluated computationally. Both the SD and HPW models describe diffusion in a planar membrane. However, membrane inclusions may generate distortions of the membrane's shape [9–11]. A recent model by Naji, Levine, and Pincus (NLP) [12] considers protrusions as generating additional dissipation in the bulk fluid, leading to an effective translational drag:

$$\Lambda_{T,\mathrm{eff}} = \Lambda_T + c\eta_w a(\Lambda_T)^{-1}. \tag{3}$$

The parameter c is, roughly, the ratio of the volume of bulk fluid displaced by the membrane deformation to a^3. High values of c, then, indicate that the presence of the membrane inclusion is leading to large out-of-plane

membrane deformations, while low values correspond to relatively smaller membrane deformations.

In conventional microrheology, the viscosity of Newtonian fluids is typically extracted from measurements of (just) the translational diffusion coefficient D_T of tracer particles [13,14]. This diffusion coefficient, the temperature and the tracer's radius can then be used to determine the viscosity of the fluid by using an appropriate model. For 3D fluids, the radius a is typically taken to be the tracer particle radius, though there are situations in which this is a poor assumption due to interactions between the particle and its surroundings [15]. For membranes, it is especially dangerous to assume that the effective radius of the diffusing object is identical to the radius of a membrane-bound tracer. Unless using phase-separated lipid domains as tracers [2,16,17], in which case the tracer radius equals the domain radius, the tracked particles must be peripherally bound to the lipid bilayer, for example, by a protein-lipid linkage. The number of lipid links is generally not easily controlled, and could range from one lipid (an area of approximately 70 Å^2 [18]) to an upper limit set by the tracer surface area. Moreover, it would not be surprising if the binding of a colloidal particle induced distortions of the membrane topography, further impacting the effective size of the diffusing object. We address these issues by measuring the rotational diffusion coefficients (D_R) of our membrane-bound tracers in tandem with their translational diffusion coefficients (D_T). These two measurements allow determination of the two unknown quantities, namely, the inclusion radius a and the membrane viscosity η_m, via the SD, HPW, or NLP relations.

Experimentally, we make use of planar bilayers spanning apertures in supports, also known as black lipid membranes (BLMs). The geometry conveniently confines tracer motion to the focal plane of our microscope, and the lack of a support eliminates frictional coupling between the membrane and solid or polymeric substrates [19]. The bilayers are formed using Langmuir-Schaefer deposition [20] from lipid monolayers at air-water interfaces, composed of a majority (typically 98%) of a single lipid species, for instance 1, 2-dioleoyl-sn-glycero-3-phosphocholine (DOPC), with a small percentage of fluorescent lipid probes for visualizing the membrane (Texas Red DHPE) and lipids with biotinylated head groups. (See Supplemental Material [21] for details of the membrane preparation and lipid compositions.) The membranes span 100 μm diameter apertures in hydrophobically coated gold transmission electron microscope grids. This diameter is large compared to the physical tracer size, the effective tracer radii noted below, and the length scale set by the ratio of (expected) 2D to 3D viscosities $\eta_m/\eta_w \approx 1$ μm.

The biotinylated lipids in the membrane are bound by neutravidin-coated fluorescent microspheres of radius 100 nm. These in turn bind 100 nm biotinylated fluorescent microspheres (Fig. 1), forming an extended unit whose

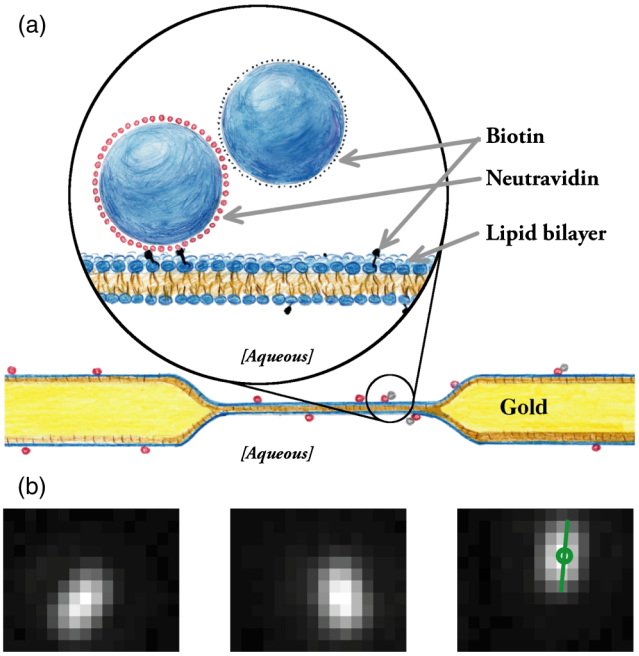

FIG. 1 (color online). Experimental setup. (a) Schematic of a membrane spanning an aperture. Fluorescent microspheres are associated with the membrane via a protein linkage, including some that are also bound with other microspheres to form the nonspherical tracers considered in the text. (b) Fluorescence images of one microsphere pair, separated by 0.3 sec. Both rotational and translational motion are apparent as the tracer thermally diffuses. The final image shows the best-fit center and orientation of the tracer. Scale: 0.123 μm/pixel.

orientation as well as position can be discerned in CCD images. Fluorescence images of beads were captured at 10 to 40 frames/ sec, and analyzed to give particle locations and orientations with an estimated precision of 1.2 nm and 0.022 radians, which yield average uncertainties of 6.3 nm^2/s for D_T and 7.2×10^{-4} rad^2/s for D_R, both of which are negligible compared to the statistical spread in the data. Image analysis methods and tests of accuracy using simulated CCD images [22] are described in the Supplemental Material [21]. All experiments were carried out at room temperature (24 ± 1°C).

The small tracer size helps ensure that tracer motion is dominated by the mechanics of the membrane rather than dissipation in the bulk fluid. For an expected membrane viscosity of, roughly, $\eta_m \approx 3 \times 10^{-9}$ Pa · s · m [6], the Stokes drag for translation in the bulk for a bead of radius $\approx$100 nm is an order of magnitude smaller than the Saffman-Delbrück drag Λ_T for a 100 nm disk; the same relative scale holds for rotation. Furthermore, with the above values, the dimensionless size parameter $\epsilon \approx 0.1$. Therefore, though we perform calculations using the full HPW model, we expect our system to occupy the regime of validity of the SD relations. Note also that, though the HPW and SD models describe the diffusion of cylinders

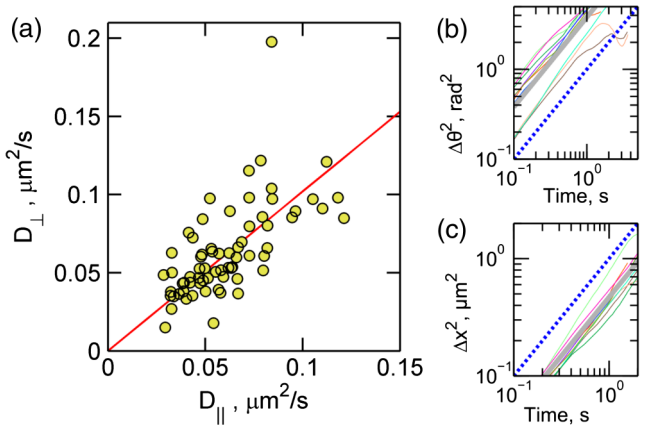

FIG. 2 (color online). Diffusive behavior of tracers at DOPC bilayers. (a) Diffusion coefficients for motion parallel ($D_\parallel$) and perpendicular ($D_\perp$) to the tracer long axis. The best fit line, shown in red, has slope $B = 1.03 \pm 0.04$, indicating isotropic diffusion. (b) and (c) Translational and angular mean square displacements versus time for several tracers. The average is shown as a thick gray line, while a dotted line with slope = 1 (expected for purely diffusive motion) is shown as a guide to the eye.

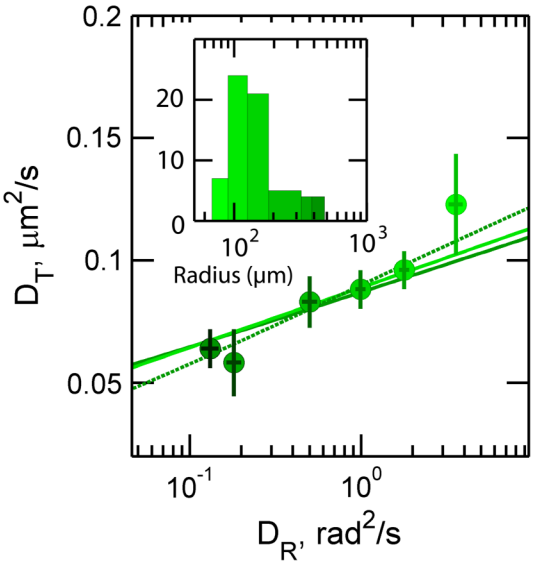

FIG. 3 (color online). Effective inclusion radius and viscosity of a DOPC bilayer. (Main panel) Translational and rotational diffusion coefficients. Each data point is the average of 4 to 24 individual tracer measurements, with the error bars indicating the standard deviations. Decreasing inclusion radius size is indicated by progressively lighter shades of green. The curves are best-fit constant-viscosity contours determined by the SD (light green, solid), the HPW (dark green, solid), and NLP (dark green, dashed) models. (Inset) Histogram of effective tracer inclusion radii on log-linear axes. The bins correspond to the data points in the main panel, with radii obtained using the SD model, and placed such that the left-hand edge of the bin corresponds to the largest inclusion radius in its set. Though peaked near the microsphere radius of 100 nm, much larger inclusion radii are evident.

incorporated into membranes, the diffusion of membrane inclusions in this regime is largely insensitive to protrusions [23].

We are able to observe the translational and rotational diffusion of membrane-anchored particle pairs (Fig. 1). The elongated form of the composite paired tracer does not bias the tracers' trajectories. Decomposing the translational diffusion into components along ($D_\parallel$) and perpendicular ($D_\perp$) to the ellipse major axis, we find that $D_\parallel = BD_\perp$ with $B = 1.03 \pm 0.04$ [Fig. 2(a)], implying that the diffusing object can be treated effectively as an isotropic membrane inclusion. As we would expect from the dominance of the membrane drag compared to the bulk noted above, and from the lack of binding between the secondary beads and the bilayer, it appears that the tracer motion is dominated by the diffusion of a region of anchored lipids diffusing within the bilayer and not by the size and shape of the tracer pair. We find that the mean-squared translational and rotational displacements are each linear in time over experimentally accessible time scales [Fig. 2(b)], indicative of Newtonian fluid dynamics, and thereby allowing application of the SD and HPW models.

We observe a spread of D_T and D_R values within and among lipid bilayers of identical composition. Applying the SD relations yields a wide range of effective radius (a) values (Fig 3, inset). The mean inclusion radius, 170 nm, is orders of magnitude larger than the radius of single lipids (0.5 nm [18]), and is about twice as large as the 100 nm radius of the primary membrane-linked microspheres. The distribution shows a long tail with some effective radii exceeding 500 nm. On the other end, we do not find radii much smaller than 50 nm, indicating that each neutravidin-coated microsphere is anchored to the membrane at several binding sites.

Each of the models of membrane viscosity we consider describes a relationship between D_R and D_T for a given viscosity. This relationship can be used to construct contours of constant viscosity on D_R-D_T axes (Fig. 3). If a particular model describes the D_R and D_T measurements well, the measured values for individual tracers should collapse on to one of these contours. We find that the SD model is a fair fit to the data (Fig. 3), yielding a best-fit viscosity of $15.3 \pm 3.4 \times 10^{-9}$ Pa · s · m for DOPC bilayers. The goodness of fit (reduced χ^2) of the SD model to our data is 0.41. The full HPW model performs similarly, with a viscosity of $15.9 \pm 2.3 \times 10^{-9}$ Pa · s · m, and reduced $\chi^2 = 0.48$. It is reasonable to speculate that our tracers may deform the membranes to which they are associated. We therefore also fit our data to the NLP model. This achieves a closer fit (reduced $\chi^2 = 0.28$), with viscosity $13.1 \pm 2.6 \times 10^{-9}$ Pa · s · m, but at the expense of the additional parameter c. One would expect $c^{1/3}$, the effective rescaling of the radius due to deformation, to be of order 1. We indeed find that $c^{1/3} = 3.0 \pm 0.5$.

To evaluate the robustness of our approach for measuring membrane viscosity, we examined another lipid that, like DOPC, is in a fluid (L_α) phase at room temperature: 1,2-di-O-tridecyl-sn-glycero-3-phosphocholine (13:0 PC) [24]. Fluorescence recovery after photobleaching measurements (performed as in [25]) give similar lipid translational diffusion coefficients for the two species: $D_{\text{lipid}} = 3.4 \pm 2.3\ \mu\text{m}^2/\text{s}$ for 13:0 PC bilayers and $D_{\text{lipid}} = 4.1 \pm 1.2\ \mu\text{m}^2/\text{s}$ for DOPC bilayers. Unlike DOPC, 13:0 PC is a saturated lipid, and has a shorter acyl chain length (13 carbon atoms, compared to 18 for DOPC). Viscosity measurements for 13:0 PC (Fig. S2 [21]) give $14.7 \pm 6.9 \times 10^{-9}$ Pa · s · m using the HPW model ($\chi^2 = 3.4$), or $10.4 \pm 4.8 \times 10^{-9}$ Pa · s · m ($\chi^2 = 1.8$) using the NLP model ($c^{1/3} = 3.8 \pm 1.3$). These viscosities are similar to those we measure for DOPC. Notably, using lipid radius $a = 0.5$ nm and $D_{\text{lipid}} = 3\ \mu\text{m}^2/\text{s}$ gives a membrane viscosity of 1×10^{-10} Pa · s · m, 2 orders of magnitude smaller than that measured above. This is not surprising; it has long been known that hydrodynamic treatments fail at molecular scales, and that diffusing lipids experience an effectively lower viscosity than do embedded proteins or other larger objects [26].

The viscosity values we observe are larger than those reported for fluid phases in membranes exhibiting cholesterol-dependent phase separation, derived by examining the diffusion of domains of one phase in another [2,16,17], or by measuring the shape fluctuations of domain boundaries [27]. For liquid-disordered (L_D) phases, values of $(3.3 \pm 1.1) \times 10^{-9}$ [6] and $(5.4 \pm 1.4) \times 10^{-9}$ [28] Pa · s · m have recently been reported. There are fewer measurements of the viscosity of homogeneous (not phase-separated) fluid bilayers, and these, prior to the method introduced here, involve complex, model-dependent analyses. Dimova *et al.* examine the gravity-driven fall of a microparticle along the surface of a giant lipid vesicle, the hydrodynamic interactions between which are computed to give a two-dimensional viscosity of $(3 \pm 0.9) \times 10^{-9}$ Pa · s · m for SOPC (1-stearoyl-2-oleoyl-sn-glycero-3-phosphocholine) [29]. For DOPC, which differs by a single double bond in one of the eighteen-carbon acyl chains, Herold *et al.* report $(5.9 \pm 0.2) \times 10^{-10}$ Pa · s · m based on the Brownian motion of absorbed DNA, whose radii of gyration are estimated from comparisons of their diffusion coefficients with those of colloidal tracer particles [30]. There are several possible reasons for the ≈10× difference between the viscosity that we measure and those reported for other fluid membranes: multicomponent, phase separated membranes may simply have a lower viscosity than the phosphatidylcholine membranes used in this study; the BLMs examined here may not consistently be pure lipid bilayers, due to retention of solvent during their formation (see Supplemental Material [21]); membrane tension in the edge-adhered BLM geometry may differ considerably from that of lipid vesicles, altering the membrane viscosity. While developing experiments to investigate these topics is likely to yield future insights, a question of greater importance is whether our approach can reveal *alterations* in membrane rheology driven by membrane-active proteins.

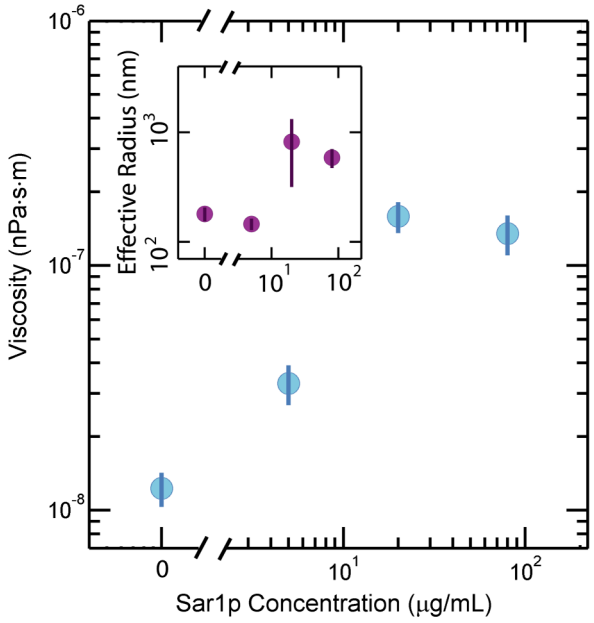

FIG. 4 (color online). Membrane viscosity measured at different concentrations of the trafficking protein Sar1p on a log-log scale. The plot shows the mean and standard error of viscosity values determined by fitting individual paired-tracer diffusion coefficients to the HPW model, at each protein concentration examined. Inset: The effective radius for the same data, also on a log-log scale.

Proteins that are actively involved in reshaping membranes, generating curvature in contexts such as cargo trafficking, filopodial extension, and mitosis [31–33], form a particularly interesting class of macromolecules in which to uncover previously unknown couplings to membrane viscosity. We focus on the vesicle trafficking protein Sar1p, a 21 kDa protein with an *N*-terminal amphipathic alpha helix that anchors it to lipid membranes [34–36]. Prior experiments have shown that Sar1p dramatically lowers the bending rigidity of lipid bilayers [37,38], leading to the open question of whether its influence also alters the in-plane viscosity. Measuring tracer diffusion in BLMs with the same endoplasmic-reticulum-mimic lipid composition and similar range of Sar1p concentration ([Sar1p]) as previously examined [37–39], we find a large drop in diffusion coefficients as a function of [Sar1p] (Fig. S3, [21]). Separating the roles of effective radius and membrane viscosity, we find an increase in a of ≈4.5×, and a dramatic increase in η_m of more than an order of magnitude (Fig. 4). Notably, the lipid diffusion coefficient is unaffected by Sar1p [40], again highlighting that the viscosity experienced at molecular length scales can differ greatly

from its effective value for larger objects. While a mechanistic explanation of the influence of Sar1p on measured viscosity is beyond the scope of this work, we note that Sar1p's reduction of the membrane bending modulus leads to enhanced topographic fluctuations [38], which may obstruct lateral motion. Notably, budding transport vesicles (formed by Sar1p and other proteins) are of similar 10–100 nm size as our tracers and their effective radii, suggesting that Sar1p's effect on viscosity at this scale can affect the dynamics of vesicle trafficking.

The results presented above demonstrate a microrheological method that can robustly be applied to fluid membranes, including membranes with bound proteins. Furthermore, since our method requires only that the membrane incorporate biotinylated lipids to contruct a tracer linkage, different model systems (e.g., supported bilayers, multilayers, and giant unilamellar vesicles) could be studied using the same approach. An important conclusion that can be drawn from our measurements is that the linkage between membrane and tracer can be nontrivial. Finally, we note that our discovery that the trafficking protein Sar1p dramatically increases large-scale membrane viscosity opens the door to a wide range of studies on the impact of proteins upon membrane rheology.

We thank John Toner and Eric Corwin for useful discussions, and acknowledge support from NSF Grants No. 1006171 (R. P., T. T. H., S. Q. K.), No. 0742540 (T. T. H.), and No. 1062512 (M. K. B., M. C. W.).

*raghu@uoregon.edu

[1] G. Vereb, J. Szöllősi, J. Matkó, P. Nagy, T. Farkas, L. Vígh, L. Mátys, T. A. Waldmann, and S. Damjanovich, Proc. Natl. Acad. Sci. U.S.A. **100**, 8053 (2003).
[2] P. Cicuta, S. L. Keller, and S. L. Veatch, J. Phys. Chem. B **111**, 3328 (2007).
[3] N. Oppenheimer and H. Diamant, Phys. Rev. Lett. **107**, 258102 (2011).
[4] J. T. Groves and J. Kuriyan, Nat. Struct. Mol. Biol. **17**, 659 (2010).
[5] D. A. Jans, *The Mobile Receptor Hypothesis: The Role of Membrane Receptor Lateral Movement in Signal Transduction* (Chapman & Hall, Austin, 1997).
[6] C. Stanich, A. Honerkamp-Smith, G. Putzel, C. Warth, A. Lamprecht, P. Mandal, E. Mann, T. Hua, and S. Keller, Biophys. J. **105**, 444 (2013).
[7] P. Saffman and M. Delbrück, Proc. Natl. Acad. Sci. U.S.A. **72**, 3111 (1975).
[8] B. D. Hughes, B. A. Pailthorpe, and L. R. White, J. Fluid Mech. **110**, 349 (1981).
[9] I. Koltover, J. O. Raedler, T. Salditt, K. J. Rothschild, and C. R. Safinya, Phys. Rev. Lett. **82**, 3184 (1999).
[10] R. N. Frese, J. C. Pàmies, J. D. Olsen, S. Bahatyrova, C. D. van der Weij-de Wit, T. J. Aartsma, C. Otto, C. N. Hunter, D. Frenkel, and R. van Grondelle, Biophys. J. **94**, 640 (2008).
[11] T. Baumgart, S. T. Hess, and W. W. Webb, Nature (London) **425**, 821 (2003).
[12] A. Naji, A. Levine, and P. Pincus, Biophys. J. **93**, L49 (2007).
[13] T. G. Mason and D. A. Weitz, Phys. Rev. Lett. **74**, 1250 (1995).
[14] T. G. Mason, K. Ganesan, J. H. van Zanten, D. Wirtz, and S. C. Kuo, Phys. Rev. Lett. **79**, 3282 (1997).
[15] B. D. Hoffman and J. C. Crocker, Methods Cell Biol. **83**, 141 (2007).
[16] E. Petrov, R. Petrosyan, and P. Schwille, Soft Matter **8**, 7552 (2012).
[17] A. R. Honerkamp-Smith, F. G. Woodhouse, V. Kantsler, and R. E. Goldstein, Phys. Rev. Lett. **111**, 038103 (2013).
[18] D. Marsh, *Handbook of Lipid Bilayers* (CRC Press, Boca Raton, 2013).
[19] R. Macháň and M. Hof, Biochim. Biophys. Acta **1798**, 1377 (2010).
[20] G. Barnes and I. Gentle, *Interfacial Science: An Introduction* (Oxford University Press, Oxford, 1995).
[21] See Supplemental Material at http://link.aps.org/supplemental/10.1103/PhysRevLett.112.188101 for information regarding sample preparation, and also descriptions of error analysis for the particle localization methods used in the experiments.
[22] R. Parthasarathy, Nat. Methods **9**, 724 (2012).
[23] M. Sickert, F. Rondelez, and H. Stone, Europhys. Lett. **79**, 66 005 (2007).
[24] J. R. Silvius, *Thermotropic Phase Transitions of Pure Lipids in Model Membranes and Their Modifications by Membrane Proteins* (John Wiley & Sons, New York, 1982).
[25] C. W. Harland, D. Rabuka, C. R. Bertozzi, and R. Parthasarathy, Biophys. J. **94**, 4718 (2008).
[26] W. Vaz, R. Clegg, and D. Hallman, Biochemistry **24**, 781 (1985).
[27] B. A. Camley and F. L. H. Brown, Phys. Rev. Lett. **105**, 148102 (2010).
[28] A. R. Honerkamp-Smith, B. B. Machta, and S. L. Keller, Phys. Rev. Lett. **108**, 265702 (2012).
[29] R. Dimova, C. Dietrich, A. Hadjiisky, K. Danov, and B. Pouligny, Eur. Phys. J. B **12**, 589 (1999).
[30] C. Herold, P. Schwille, and E. P. Petrov, Phys. Rev. Lett. **104**, 148102 (2010).
[31] H. McMahon and J. Gallop, Nature (London) **438**, 590 (2005).
[32] J. Zimmerberg and M. Kozlov, Nat. Rev. Mol. Cell Biol. **7**, 9 (2006).
[33] R. Parthasarathy and J. Groves, Soft Matter **3**, 24 (2007).
[34] A. Nakańo and M. Muramatsu, J. Cell Biol. **109**, 2677 (1989).
[35] C. Barlowe, C. d'Enfert, and R. Schekman, J. Biol. Chem. **268**, 873 (1993).
[36] M. Lee, L. Orci, S. Hamamoto, E. Futai, M. Ravazzola, and R. Schekman, Cell **122**, 605 (2005).
[37] E. Settles, A. Loftus, A. McKeown, and R. Parthasarathy, Biophys. J. **99**, 1539 (2010).
[38] A. Loftus, S. Noreng, V. Hsieh, and R. Parthasarathy, Langmuir **29**, 14 588 (2013).
[39] K. Matsuoka, L. Orci, M. Amherdt, S. Bednarek, and S. Hamamoto, Cell **93**, 263 (1998).
[40] A. F. Loftus, V. Hsieh, and R. Parthasarathy, Biochem. Biophys. Res. Commun. **426**, 585 (2012).